Article ID: 1006-8775(2015) 01-0023-11

COMPARATIVE ANALYSIS OF THE INTENSIFYING AND WEAKENING LANDFALL TROPICAL CYCLONES DURING EXTRATROPICAL TRANSITION OVER CHINA

LI Kan (李 侃)[1,2], XU Hai-ming (徐海明)[2,3]
(1. Pingxiang Meteorological Bureau of Jiangxi Province, Pingxiang 337002 China; 2. College of Atmospheric Science, NUIST, Nanjing 210044 China; 3. Key Laboratory of Meteorological Disaster of Ministry of Education/Nanjing University of Information Science & Technology, Nanjing 210044 China)

Abstract: Based on the Tropical Cyclone (TC) Yearbooks data and JRA-25 reanalysis data from the Japan Meteorological Agency (JMA) during 1979-2008, dynamic composite analysis and computation of kinetic energy budget are used to study the intensifying and weakening TCs during Extratropical Transition over China. The TCI shows strong upper-level divergence, strengthened low-level convergence and significantly enhanced upward motion under the influence of strong upper-level troughs and high-level jets. The TCI is correspondingly intensified after Extratropical Transition (ET); TCW exhibits strong upper-level divergence, subdued low-level convergence and slightly enhanced upward motion under the influence of weak upper-level troughs and high-level jets. It then weakens after ET. The increase (decrease) of the generation of kinetic energy by divergence wind in TCI (TCW) at low level is one of the major reasons for TCI's intensification (TCW's weakening) after transformation. The generation of kinetic energy by divergence wind is closely related to the development of a low-level baroclinic frontal zone. The growth of the generation of kinetic energy by rotational wind in TCI at upper level is favorable for TCI's maintenance, which is affected by strong upper-level troughs. The dissipation of the generation of kinetic energy by rotational wind in TCW at upper level is unfavorable for TCW's maintenance, which is affected by weak upper-level troughs.

Key words: tropical cyclone; intensification during extratropical transition; weakening during extratropical transition; dynamic composite analysis; kinetic energy budget
CLC number: P444 **Document code:** A

1 INTRODUCTION

Tropical cyclones (TCs) generally generate and develop over tropic oceans and often land at low-latitude coastwise areas. However, TCs that move poleward into mid-latitude areas frequently undergo extratropical transition (ET) processes which are accompanied with significant changes of structure, translation speed and intensity and bring about disastrous weather such as strong precipitation, gale, sea swell, et al. (Jones et al.[1]; Zhao et al.[2]; Liang et al.[3]). For the study of the ET, Foley and Hanstrum[4] and Klein et al.[5] consider the in teraction between TC and mid-latitude baroclinicity systems to be one of the main reasons for the disappearance of TC's symmetrical structure and the evolvement of ET. Harr and Elsberry[6-7] also found that the ET of TCs in the western North Pacific is closely related with two kinds of typical mid-latitude circulation (of either the northwest or northeast pattern). The study of Ritchie and Elsberry[8] shows that the phase between TCs and mid-latitude troughs is the key factor in forecasting the intensity of ET. Many studies about the interaction between TCs and mid-latitude baroclinic systems have been presented by foreign scholars, but most of their findings discuss just the ET process in the Sea of Japan and the North Atlantic, there has been little research on the ET process in China. In recent years, more attention has been paid by domestic researchers on the ET issue in pace with the exhaustive studies of the change of TC intensity over the western North Pacific (Duan et al.[9]). Zhu et al.[10] suggested that low-level warm advection, divergence associated with high-level jet streams and upper-level advection of vorticity are important physical factors in the intensifying typhoon Winnie (9711) during the ET over China. Their numerical simulations also indicated that the transition and re-intensification of Winnie after the ET are closely linked with latent heat by precipitation (Zhu et al.[11]). According to Li et al.[12], Winnie's re-intensification after ET is related to the interactions between typhoon remnant circulation and low-level frontal zone and the downward transportation of potential vorticity anomaly from the upper troposphere. The stronger an upper trough is, the faster Winnie re-intensifies (Li et al.[13]). Further diagnostic analysis

Received 2013-09-04; **Revised** 2014-10-24; **Accepted** 2015-01-15
Foundation item: National Key Technology R&D Program (2012BAC22B03); NSFC General Program (41275094)
Biography: LI Kan, master of meteorology, primarily undertaking research on short-range forecast and research on tropical cyclones.
Corresponding author: LI Kan, e-mail: litianhao1985@126.com

of the frontogenesis phe nomenon which occurs in the circulation of Winnie during its ET and re-intensification process finds that the intensification of the remnant of Winnie looks like an extratropical cyclone developing in the surface frontal zone (Li et al.[14]). The spatio-temporal distribution characteristics of the extratropical transition of TCs over the Northwest Pacific during 1961 to 2000 are investigated based on the method of climatology (Zhong et al.[15]). Domestic studies on the ET process of TCs landing on China have been conducted, but with the focus mostly on cases like Typhoon Winnie only and with statistical analyses mainly taking the season and location of ET into consideration.

What are the differences between an intensifying TC and a weakening TC during ET over China (referred to as TCI and TCW respectively hereafter)? What are the effects of environment on TCI and TCW? What are the distinctions of energy budget between them? Research on those issues can enhance the understanding of the ET process. In this work, statistics of TCs that underwent ET during 1979-2008 over China are presented and composite analysis is used to contrast TCI and TCW in order to avoid the differences among cases and reveal the main features of the ET system better.

2 DATA, METHODOLOGY AND EXAMPLE

In the subsequent section, the TC track and intensity data are supplied from the 6-hourly best track data, which include the centre location, minimum pressure and maximum wind speed by Japan Meteorological Agency (JMA). The environment field of TCI and TCW will be composed by using a JRA-25 reanalysis global grid dataset with a horizontal resolution of 1.25° × 1.25° at 23 mandatory pressure levels available four times daily (Onogi et al.[16]) and utilizing a dynamic synthesis method which follows with the TC center (Li et al.[17]). Five points of time are chosen for the composite analysis, which are the ending time of ET, 12 h and 24 h prior to the ET, and 12 h and 24 h after it.

Hart[18] pointed out that the occurrence of ET is actually due to the evolution from a warm core of a TC to a cold core of an extratropical cyclone when the TC is moving poleward and interacting with middle-latitude synoptic systems. Evans and Hart [19] summarizes three objective parameters for determination of ET events through studying 61 TCs that underwent ET in the Atlantic from 1979 to 1993.

$$B = h\left(\overline{Z_{600} - Z_{900}}\Big|_{\mathrm{R}} - \overline{Z_{600} - Z_{900}}\Big|_{\mathrm{L}}\right) \quad (1)$$

$$\left.\frac{\partial(\Delta Z)}{\partial \ln p}\right|_{600\mathrm{hPa}}^{300\mathrm{hPa}} = -V_T^U \quad (2)$$

$$\left.\frac{\partial(\Delta Z)}{\partial \ln p}\right|_{900\mathrm{hPa}}^{600\mathrm{hPa}} = -V_T^L \quad (3)$$

where B is the parameter for thermal asymmetry of the TC, $-V_T^U$ is the parameter of upper-level thermal wind and $-V_T^L$ that of low-level thermal wind. In Exp. (1), Z is the geopotential height, R(L) represents the right (left) side of the TC movement direction, and the overbar indicates the spatial mean for a 500-km radius over the left (right) semicircle on the right and left side along the TC movement direction, and h is a value +1 in the Northern Hemisphere and a value -1 in the Southern Hemisphere. In Exps. (2) and (3), $\triangle Z$ is $Z_{\max}-Z_{\min}$, evaluated within a radius of 500 km around the TC center and p is the pressure.

It was once suggested by Klein el al.[5] that the ET of a TC includes two stages in a broad sense: transition stage and re-development stage in which the TC may weaken or re-intensify. Following the statistics by Evans and Hart [19], when the TC begins the ET, B>10 and the ET is defined to end, which also means the beginning of the re-development phase, when $-V_T^U$ and $-V_T^L$ change from positive to negative. The ending time of transition phase is labeled as Te in this paper; Te-12 and Te-24 respectively mean 12 h and 24 h prior to Te, which are analogous with Te+12 and Te+24. Zhang et al.[20] proved that the index summarized to determine the ET of TC in the Atlantic by Hart et al. is also applicable to the ET process of TC Haima landing in China. Wang and Song [21] calculated three parameters of TC in Western Pacific with the JRA-25 reanalysis dataset from 1979 to 2007 and evaluated these parameters using the ET data recorded by TC Yearbooks in Shanghai Typhoon Institute of the China Meteorological Administration. The results indicated that these parameters can effectually distinguish ET events in Western Pacific when B>10, $-V_T^U$<0 and $-V_T^L$<0 at the same time, useful as the optimum objective threshold for distinguishing the transition of TCs in the northwest Pacific.

Statistics determined by computing the indexes of ET and combining the ET dataset provided by Wang and Song[21] in the Northwest Pacific from 1979 to 2008 show that 30 TCs experienced ET after landfall, which accounts for about 15.23% of all TCs landing in China during the 30 years. Of the landing TCs, 16 underwent ET in mainland China, 11 in China's offshore, 2 in the sea south of Japan, and 1 in the Sea of Japan. TCI is defined as an intensifying ET case whose minimum central pressure after Te is smaller than that for Te-6. Otherwise it is defined as a TCW. There are 10 samples of TCI and 20 samples of TCW following the standard above. In order to reduce the regional differences and highlight the effect of environmental field, composite analysis was carried out with 6 TCI and 6 TCW cases in Shangdong province, Jianghuai Rivers Basin and their inshore area. Fig.1 gives the path of TCI and TCW for the time after landfall and the locations of Te are represented by the black dots.

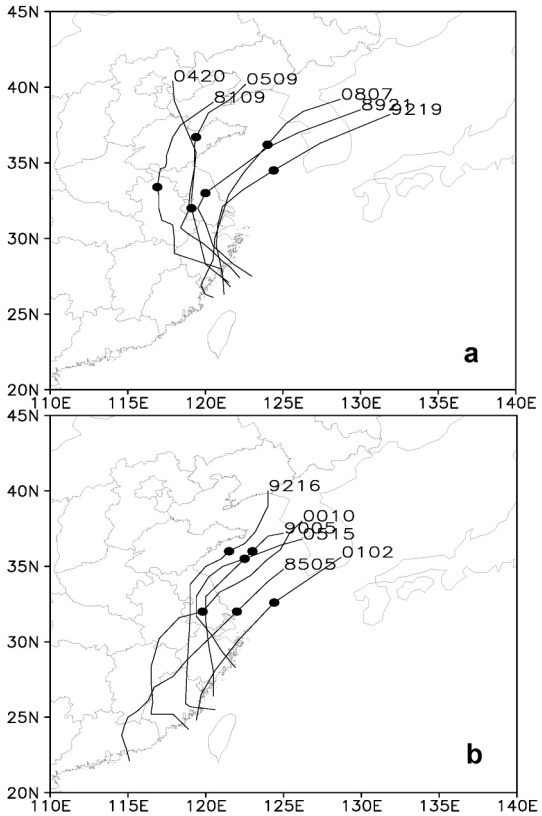

Figure 1. The paths of (a) TCI and (b) TCW after landfall. The locations of Te are represented by the black dots.

3 COMPARATIVE ANALYSIS OF THE ENVIRONMENTAL FIELDS BETWEEN TCI AND TCW

3.1 *Synoptic situation at 200 hPa and 500 hPa*

The composite field of geopotential height at 200 hPa demonstrates that the westerly troughs at the upper level are accompanied by jet streams (shadow areas with mean wind speed larger than 30 m/s in Fig. 2) before the transitions of TCI and TCW occur in mid-and higher-latitude areas. It can be seen by comparing Fig. 2a with Fig. 2c that the meridional span of TCI's upper-level circulation is wider and the trough aloft is stronger before Te. Both the TCI and TCW move northward and gradually approach the jet streams while the troughs move eastward. The supply of stronger positive vorticity (PV) advection in front of the trough delivers PV into the TC with further deepening of TCI's trough after Te, which is beneficial to the maintenance and development of TCI (Fig. 2b)[13]. Otherwise, the transport of PV advection is weaker with a shallow trough of TCW (Fig. 2d).

Zhu et al.[10] thought that the descent of the middle and upper level cold air is the key of ET. It can be seen that the temperature field falls behind the geopotential height field and the baroclinic feature is remarkable at Te from the compositing fields of temperature and height at 500 hPa (Fig. 3). The cold air intrudes southward into the circulation of TCI at the side of the

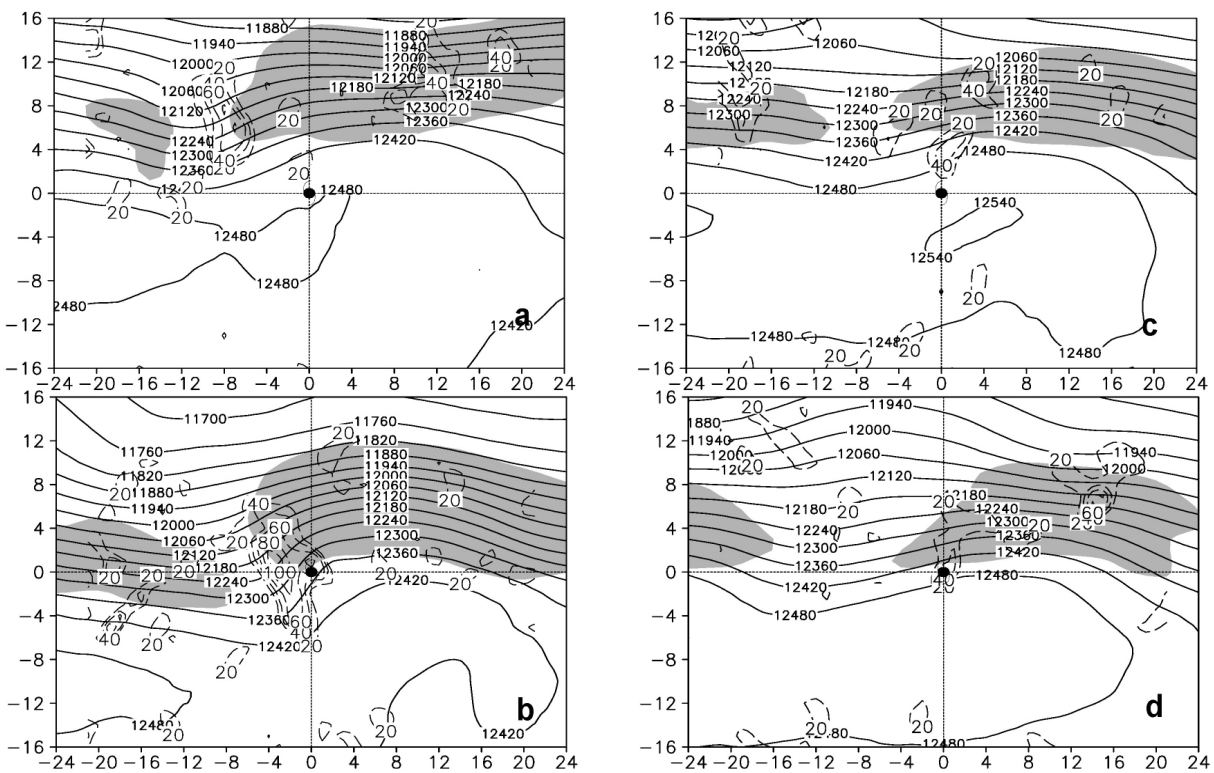

Figure 2. The geopotential height (solid line, units: gpm), PV advection (dashed line, ≥ 20× 10^{-10} s^{-2}) and high-level jet (shading, ≥ 30 m/s) of TCI (left) and TCW (right) at 200 hPa. (a, c): Te-12; (b, d): Te+12. The coordinate origin is the centre of TC (positive values are northward and eastward, and negative values are westward and southward) and the horizontal resolution is 1.25° × 1.25° (longitude by latitude), and the same below.

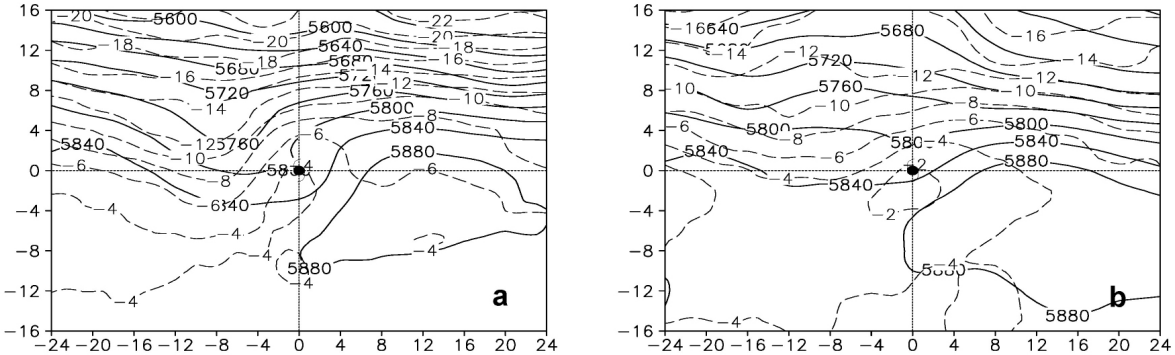

Figure 3. The geopotential height (solid line, units: gpm) and temperature (dashed line, units: ℃) of TCI (a) and TCW (b) at 500 hPa at the time of Te.

trough with the TCI's entry to the baroclinic zone (Fig. 3a), which results in the ET of TCI. A shallow short-wave trough and a weak temperature trough are located in the northwest of TCW, but the weak cold air still invades into TCW, leading to the ET of TCW (Fig. 3b).

3.2 *The distinction of divergence between TCI and TCW*

It is shown in the Fig. 2 that TCI and TCW are both located in the divergence region at the right of the entry to the high-level jet stream, according to Bosart et al.[22], and the upper-level strong divergence can intensify the medial ascending motion of TC which enhances the TC by increasing the low-level convergence. Fig. 4 gives the vertical cross sections of the divergence differences of TCI and TCW between Te-12 and Te+12 in order to further discuss the influences of the high-level jet stream on TCI and TCW. When TCI and TCW move into the divergence region at the right of the entry to the high-level jet stream, their upper-level divergence both strengthen (the divergence differences are negative at the upper level) after Te, but the upper-level divergence of TCI intensifies more obviously than TCW ($|-25\times10^{-6}\ s^{-1}|>|-15\times10^{-6}\ s^{-1}|$) and the value of divergence difference was $35\times10^{-6}\ s^{-1}$ near the low-level centre of TCI, which means the convergence of TCI enhances remarkably (Fig.4a). Otherwise, the low-level convergence of TCW weakens and changes little on the level above (Fig.4b).

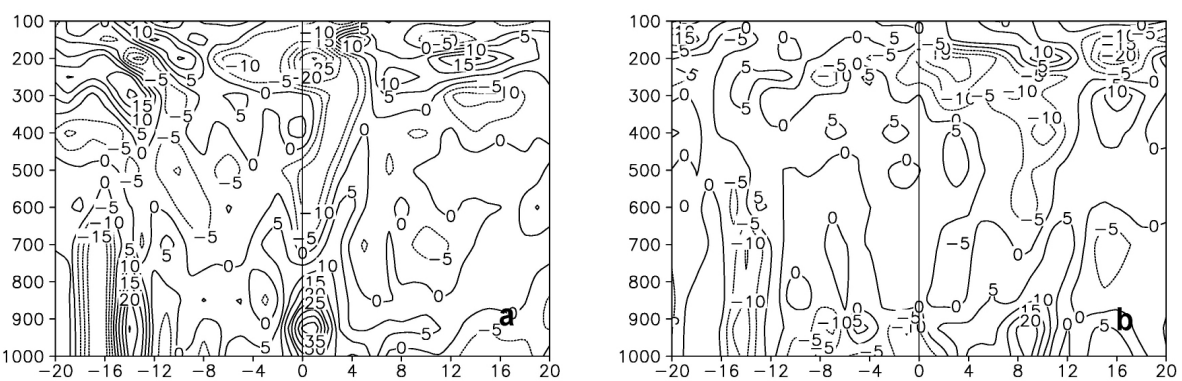

Figure 4. The zonal cross sections of the divergence (units: $10^{-6}\ s^{-1}$) differences of TCI (a) and TCW (b) between Te-12 and Te+12.

3.3 *Vertical motion of TCI and TCW*

Figure 5 illustrates the zonal cross sections of the vertical velocity differences between TCI and TCW at Te-12 and Te+12. The extreme center of middle and low-level vertical velocity is 0.6 Pa/s (Fig. 5a), which implies that the ascending motion in the vicinity of the center of TCI will be much strengthened. The ascending motion of TCW is not obvious (Fig. 5b).

4 KINETIC ENERGY BUDGET OF TCI AND TCW

The energy budget of TC is significant to its maintenance, development and declining. To further investi gate the distinctions between TCI and TCW before and after Te, comparative analysis will be carried out in the next section from the view of energy.

4.1 *The kinetic energy budget of divergent and rotational wind*

The actual wind field can be divided into divergent ($\vec{V}_D$) and rotational ($\vec{V}_R$) wind components. Pearce[23] confirmed that the generation of kinetic energy by divergent (rotational) wind is closely related to baroclinic (barotropic) process, therefore we can get a deeper understanding of the physical process of kinetic energy's

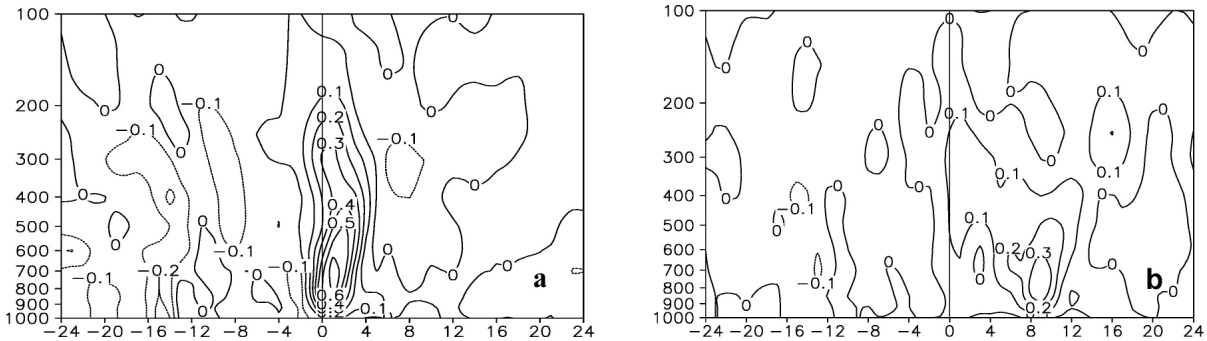

Figure 5. The same as Fig. 4 but for the vertical velocity differences (units: Pa/s).

transformation in TCI and TCW by calculating kinetic energy budget of divergent and rotational wind. The solution of divergent and rotational wind was sought following the theory of Endlich[24].

4.1.1 COMPUTATIONAL FORMULA

$$\vec{V} = \vec{V}_R + \vec{V}_D \tag{4}$$

Kinetic energy per unit mass (k) is given as in $k=\frac{1}{2}\vec{V}\cdot\vec{V}$. Application of Eq.(4) yields

$k = k_R + K_D + \vec{V}_R + \vec{V}_D$ where $k_R = \frac{1}{2}\vec{V}_R\cdot\vec{V}_R$ and $k_D = \frac{1}{2}\vec{V}_D\cdot\vec{V}_D$.

The kinetic energy of an atmospheric volume in isobaric coordinates is given by $K = \iint k$, $K_R = \iint k_R$, $K_D = \iint k_D$, where $\iint = \frac{1}{gA}\iiint dxdydp$ and A is the area of the computed domain.

Thereby rewrite $k = K_R + K_D + \vec{V}_R\cdot\vec{V}_D$ as

$$K = K_R + K_D + \iint \overrightarrow{V_R}\cdot\overrightarrow{V_D} \tag{5}$$

The budget formula (Buechler and Fuelberg[25]) of K_D and K_R are presented as follows:

$$\underset{DKD}{\frac{\partial K_D}{\partial t}} = \underset{INTD}{\iint -\overrightarrow{V_D}\cdot\frac{\partial\overrightarrow{V_R}}{\partial t}} - C(K_D,K_R) + \underset{HFD}{\iint -\nabla\cdot k\overrightarrow{V_D}} + \underset{GD}{\iint -\overrightarrow{V_D}\cdot\nabla\varphi} + \underset{VF}{\iint -\frac{\partial\omega k}{\partial p}} + \underset{DD}{\iint \overrightarrow{V_D}\cdot\vec{F}} \tag{6}$$

$$\underset{DKR}{\frac{\partial K_R}{\partial t}} = \underset{INTR}{\iint -\overrightarrow{V_R}\cdot\frac{\partial\overrightarrow{V_D}}{\partial t}} + C(K_D,K_R) + \underset{HFR}{\iint -\nabla\cdot k\overrightarrow{V_R}} + \underset{GR}{\iint -\overrightarrow{V_R}\cdot\nabla\varphi} + \underset{DR}{\iint \overrightarrow{V_R}\cdot\vec{F}} \tag{7}$$

$$C(K_D,K_R) = \iint -f\left(u_D v_R - u_R v_D\right) + \iint -\zeta\left(u_D v_R - u_R v_D\right) + \iint -\omega\frac{\partial k_R}{\partial p} + \iint -\omega\overrightarrow{V_R}\cdot\frac{\partial\overrightarrow{V_D}}{\partial p} \tag{8}$$

$C(K_D,K_R)$: the conversion between K_D and K_R;

DKD, *DKR*: K_D and K_R with time varying;

GD, *GR*: the generation of kinetic energy by divergent and rotational wind;

HFD, *HFR*: the horizontal flux divergence of K_D and K_R;

INTD, *INTR:* the interactions between K_D and K_R due to the presence of the other components;

DD, *DR:* the dissipation terms of K_D and K_R;

VF: the vertical transport of K_D.

The derivation of expression and detailed physical significance of all terms from Eq.(6) to Eq.(8) are described in detail in Buechler and Fuelberg[25]. Fig. 6 presents the relationship among them. The area of A is a square comprised of 81 grids by taking TC as the centre, which requires that 9 grids are taken respectively in the x and y coordinate axes, the horizontal spacing is 125 km and the area is 10^6 km^2.

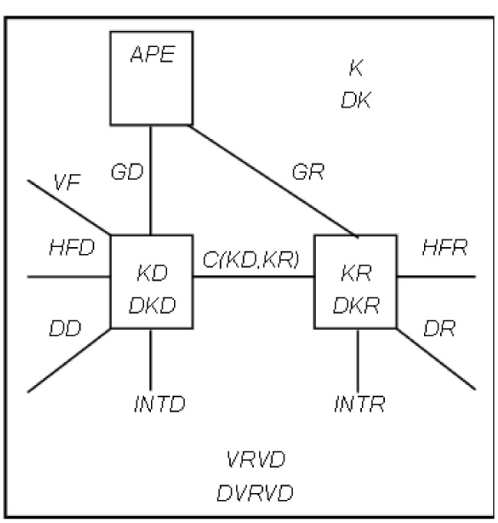

Figure 6. The schematic of kinetic energy budget where *APE* is the available potential energy.

4.1.2 KINETIC ENERGY BUDGET OF DIVERGENT AND ROTATIONAL WIND

Figure 7 illustrates the kinetic energy budget of TCI and TCW before and after Te. It can be found from Fig. 7a and Fig. 7b that the kinetic energy balance of TCI and TCW is similar and the values of all terms are close to each other at Te-12: *KR* has a larger magnitude compared with *KD* in both TCI and TCW, therefore *KR* is the dominant component of *K*, which is determined by the essential features of synoptic scale movement—quasi geostrophic motion; APE is converted to *KD* by *GD* and part of *KD* becomes *KR* through the interactions between vorticity and divergence in the case of dissipation of *GR* (which is negative). It shows, in summary, that the energy of TCI and TCW prior to Te mainly comes from the generation of baroclinic kinetic energy. The amplitude of *GD* in TCI (Fig. 7c) is larger than that of TCW(Fig. 7d) at Te+12, and correspondingly, the conversion of *KD* into *KR* is greater in TCI; Besides, the *GR* of TCI and TCW are both from negative to positive after Te, but the *GR* of TCI reaches 13.32 W/m^2, which is much greater than that of TCW (3.03 W/m^2). It indicates that the energy of TCI and TCW after Te is still mainly from the generation of baroclinic kinetic, and additionally, the generation of kinetic energy by rotational wind in TCI after Te also plays an important role in the increase of total kinetic energy. It can be discovered that *GD*, *GR*, *HFD* and *HFR* are the primary sources and sinks of kinetic energy and *C* (*KD*, *KR*) is the conversion of kinetic energy between two types of winds (Fig. 7), therefore, it is necessary to analyze their vertical distribution further.

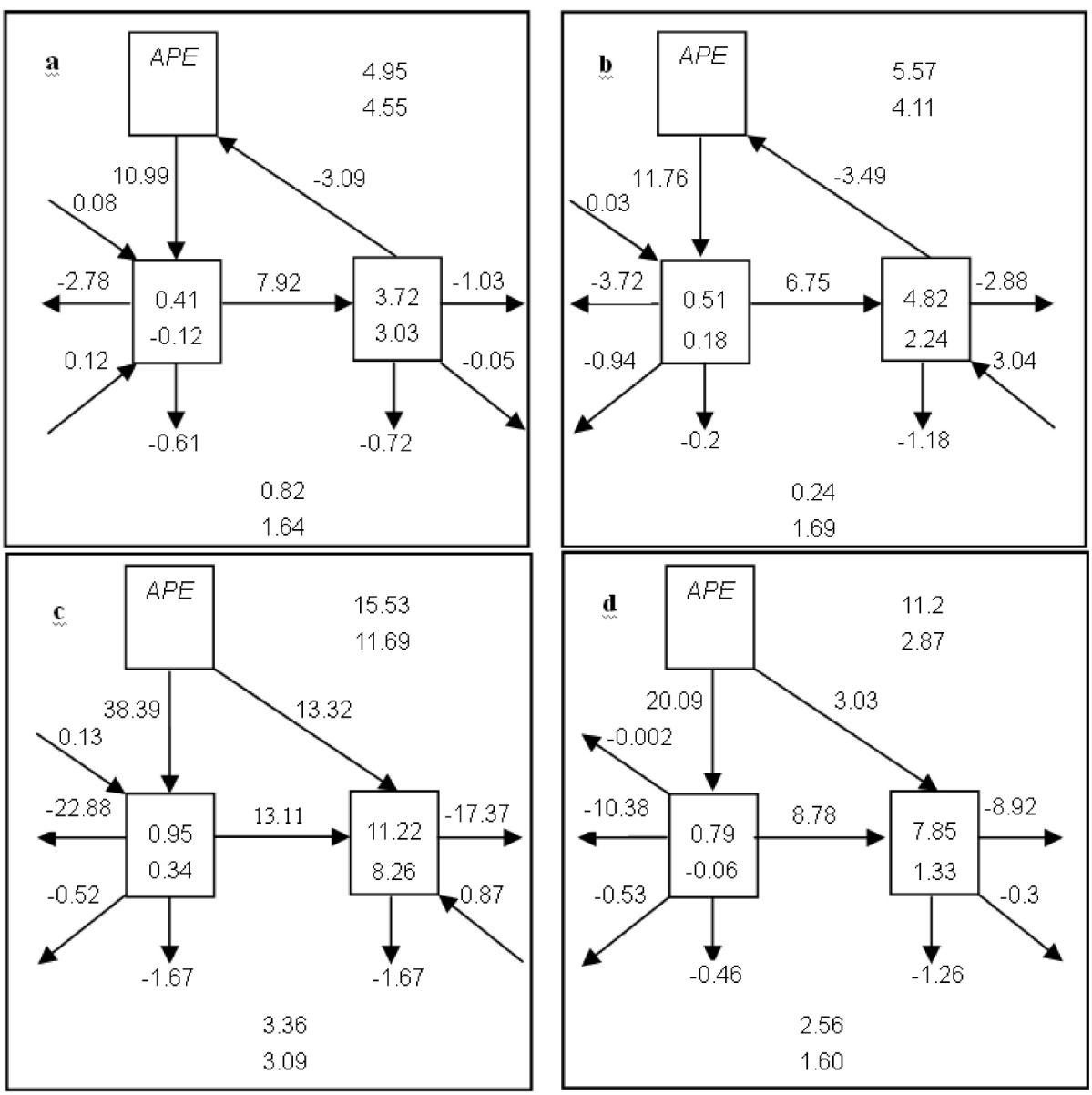

Figure 7. The kinetic energy budget of TCI (a, c) and TCW (b, d) at Te-12 (a, b) and Te+12 (c, d). The integral level is from 1 000 hPa to 100 hPa, the units of *K*, *KD*, *KR* and *VRVD* are 10^5 J/m^2 and all others are W/m^2.

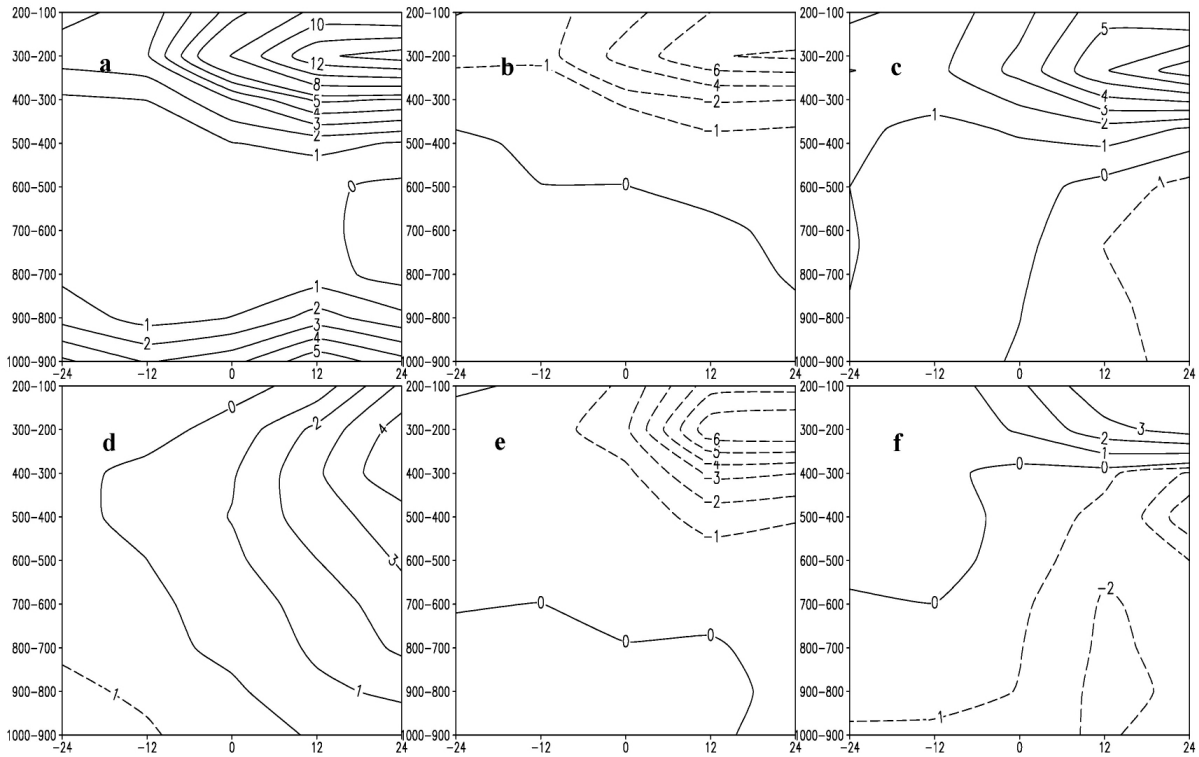

Figure 8. The time cross section of *GD* (a), *HFD* (b), *C*(*KD*,*KR*) (c), *GR* (d), *HFR* (e) and VF (f) in TCI (units: W/m^2). The negative (positive) abscissa indicates the time before (after) Te and zero is at the time of Te (units: h).

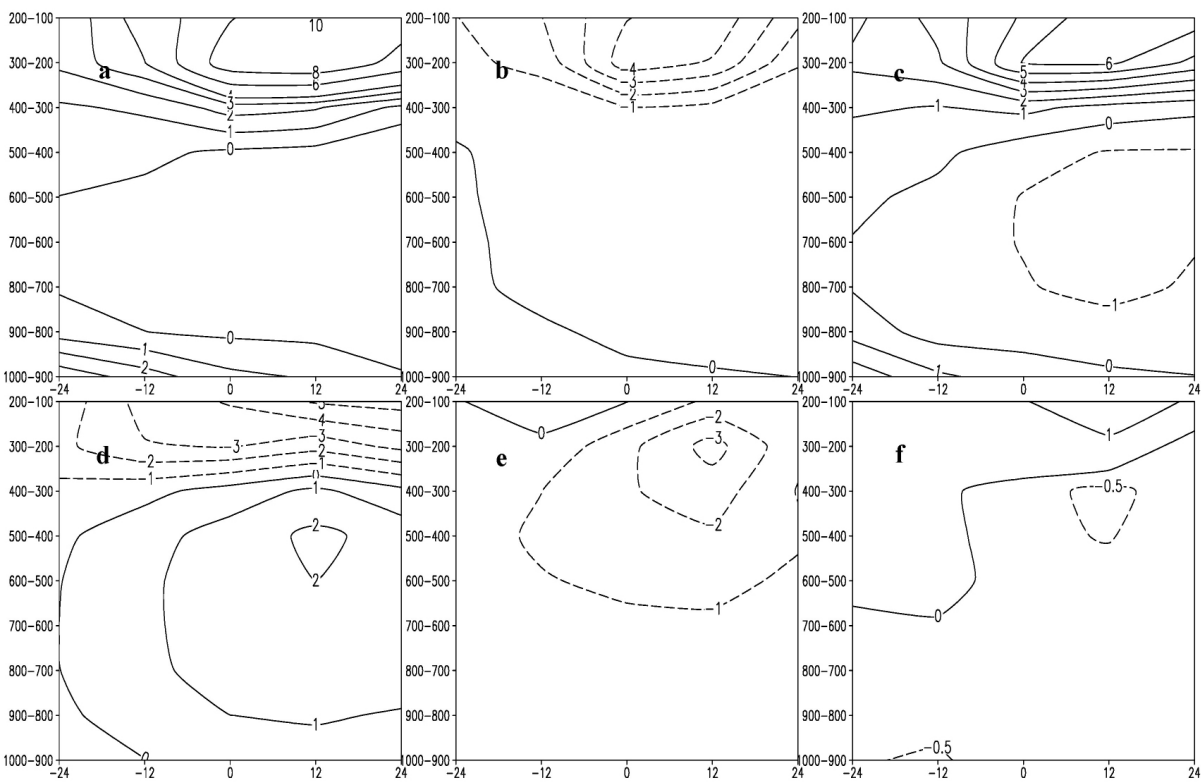

Figure 9. The same as Fig.8 but for TCW.

Figures 8 and 9 illustrate that the main input and output of *KR* and *KD* in TCI and TCW varies with time and height, which is divided into 9 equidistant layers (each layer is 100 hPa) from 1 000 hPa to 100 hPa in the vertical direction. The *GD* of TCI (Fig. 8a) and TCW (Fig. 9a) concentrate in the upper and lower tro-

posphere and their upper *GD* all grow remarkably as they are affected by the upper-level jet after Te. What differs is that the lower *GD* of TCI also has a significant increase (there is a maximum center at Te+12) unlike the decrease of low-level *GD* in TCW after Te. It can be found that the low-level *GR* of TCI and TCW are both small in Figs. 8d and 9d after Te. The analysis above shows that the low-level kinetic energy of TCI derives mainly from the kinetic manufacture of divergence wind and TCW acquires minor kinetic energy at low levels after Te. Besides, most samples of the 6 TCIs reach their minimal central pressure at Te+12 and the low pressure of 6 TCWs rose after Te, which implies that the kinetic generation of low-level divergence wind is in accordance with the intensity of the low-level cyclone, and we can confirm that the increase (decrease) of the kinetic generation by low-level divergence wind in TCI (TCW) after Te is one of the main reasons for TCI's intensification (TCW's weakening).

The upper-level kinetic energy of divergence wind produced by *GD* dissipates partially through *HFD* (Figs. 8b and 9b), one part of *KD* converts into *KR* via *C*(*KD, KR*) (Figs. 8c and 9c) in TCI and TCW after Te, and the upper-level *KR* of TCI and TCW transformed by *C* (*KD,KR*) are relatively strong and equivalent after Te. Furthermore, the low-level kinetic energy of rotational wind produced by *GR* in TCI (Fig. 8d) and TCW (Fig. 9d) is weak with the conversion of a portion of low-level *KR* into *KD* (Figs. 8c and 9c) after Te, so the *KR* of TCI and TCW are mainly focused on high levels after Te. We could find that the primary sources of *KR* in TCI and TCW come from the conversion of *KD* and the generation of *GR* (Fig. 7c and 7d). In the case of the equivalent of upper-level *KR* which is transformed by *C* (*KD,KR*) between TCI and TCW after Te, the dissipation of upper-level *KR* by *HFR* is greater in TCI (Fig. 8e and 9e), but the *KR* of TCI caused by the upper-level *GR* increases (Fig. 8d), which still makes TCI maintain strong *KR* (Fig. 7c). Moreover, the upper-level *GR* of TCW is a larger negative value which signifies the consumption of *KR*(Fig. 9d), the amplification of the total kinetic energy of rotational wind in TCW is not obvious and its growth rate remains relatively slow (Fig. 7b and 7d). In conclusion, the rise of TCI's *KR* caused by upper-level *GR* after Te implies that the atmosphere provides energy to TCI, which is favorable for the maintenance of TCI; the consumption of TCW's *KR* caused by upper-level *GR* after Te indicates the outward divergence of TCW's kinetic energy, which is disadvantageous to the sustained presence of TCW.

4.2 *The cause of KD and KR change*

Figure 10 presents the distributions of equivalent potential temperature (EPT), height and divergent wind at 850 hPa, in which the area of EPT≤ 336 K is shown

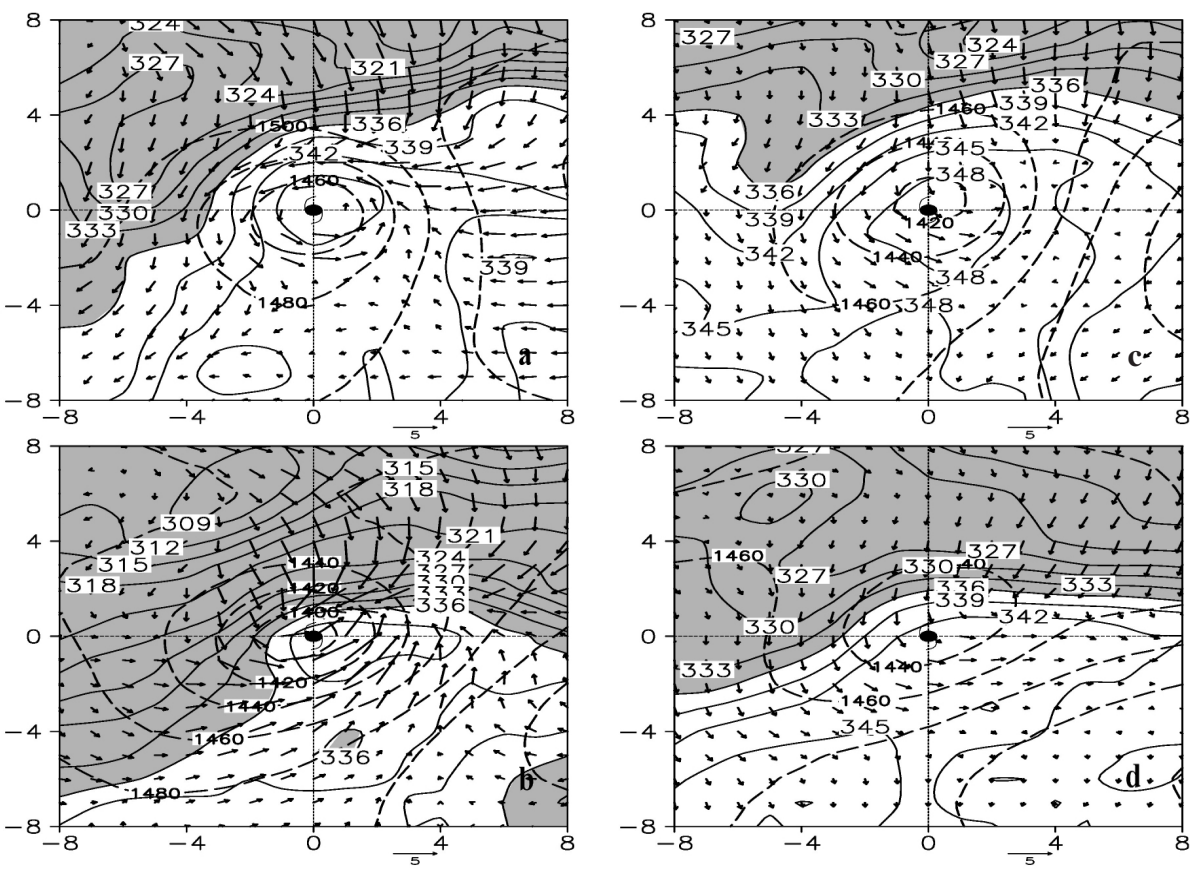

Figure 10. The equivalent potential temperature (EPT, solid line, units: K), height (dashed line, units: gpm) and divergent wind (vector arrow, units: m/s) of TCI (left) and TCW (right) at 850 hPa. (a, c): Te-12; (b, d): Te+12. The area of EPT≤ 336 K is in shadow, which is used to track cold air.

in shadow and used to track cold air. The cold air has made incursion into the northern and western peripheral circulation of TCI at Te-12 (Fig. 10a). The gradient between TCI centre and cold air strengthens such that an obvious baroclinic frontal zone is formed with further incursion of cold air into TCI at Te+12 (Fig. 10b). The incursion of cold air and the intense development of the low-level baroclinic frontal zone enhance the TCI's baroclinicity and the divergent wind remarkably (the wind vector increases next to TCI center in Fig. 10b) after Te, then enhanced divergent wind crosses the contour lines (Fig. 10b), which increases the lower *GD* of TCI evidently (Fig. 8a), and the TCI acquires strong kinetic energy of divergent wind released by baroclinic potential energy at low levels. Only mild cold air in vades into the peripheral circulation of TCW at low levels (Fig. 10c and 10d), its baroclinic frontal zone is not obvious and divergent wind changes little, and accordingly, the low-level *GD* of TCW reduces (Fig. 9a) after Te, which gives rise to the decrease of the acquired ki netic energy of divergent wind.

The above analysis makes it clear that the upper-level trough grows while the TCI is developing (Fig. 2b). It can be seen that the export of the low-level kinetic energy and import of the upper-level kinetic energy implies that there is upward transport of low-level kinetic energy of divergent wind in TCI after Te (Fig. 8f), which is the result of strong ascending motion (Fig. 5a) caused by the low-level intense convergence of TCI (Fig. 4a). Besides, the acquisition of upload kinetic energy in upper-level TCI is favorable for the development of the though (Fig. 2b) and the maintenance of divergence (Fig. 4a) at high levels. The low-level convergence attenuates (Fig. 4b) and the ascending movement does not change much (Fig. 5b) in TCW after Te, so the supply of kinetic energy from the low level to the high level is not evident (Fig. 9f). As a result, the upper-level trough of TCW dose not develop (Fig. 2d).

Figure 11 illustrates the distribution of geopotential height and rotational wind in TCI and TCW at 200 hPa. TCI's centre is not embedded in the upper-level trough and the rotational wind of TCI is still small while at Te-12 (Fig. 11a). The strong transport of PV advection in front of the trough supplies the TCI with sufficient PV with enhancement of the trough (Fig. 2b) at Te+12, which increases the upper-level rotational wind of TCI (lengthened wind vector in Fig. 11b), then its *GR* enlarges (Fig. 8d) because the rotational wind blows across the contour lines from high potential to low potential area (Fig. 11b). Correspondingly, the upper-level KR of TCI increases. The rotational wind of TCW has little alteration (Fig. 11c and 11d) due to the shallow trough and the mild supplement of PV advection (Fig. 2d). Moreover, the rotational wind of TCW blows across the contour lines from low potential to high potential area after Te, which manifests the exhaustion of upper-level *KR* (Fig. 9d). Consequently, the strong (weak) upper-level trough of TCI (TCW) is the key factor of the increase (decrease) of its upper-level *GR*.

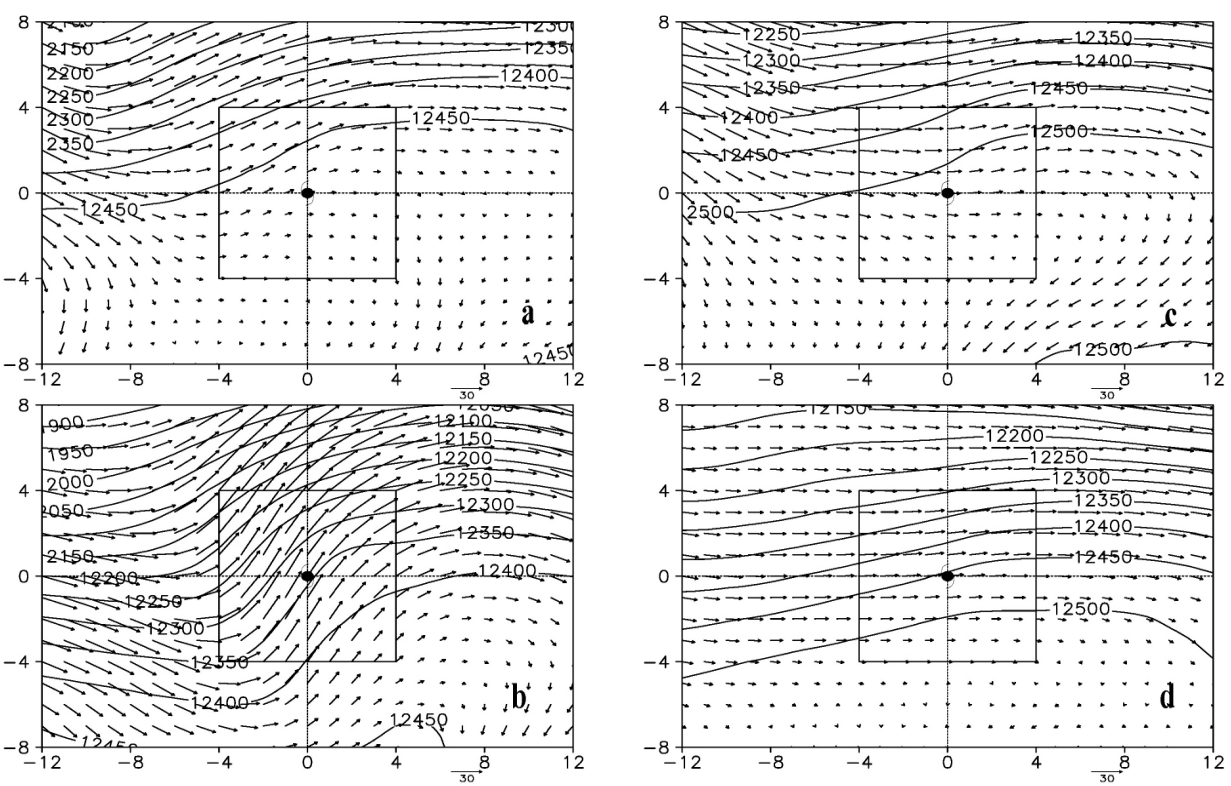

Figure 11. The geopotential height (solid line, units: gpm) and rotational wind (vector arrow, units: m/s) of TCI (left) and TCW (right) at 200 hPa. (a, c): Te-12; (b, d): Te+12. The square is the area of horizontal integral computing all terms of kinetic energy.

5 CONCLUSIONS AND DISCUSSIONS

Based on comparisons, composite analyses and calculation of kinetic energy budget are performed to study the environmental fields of TCI and TCW making landfall on China from 1979 to 2008 and a simple evolution model is obtained of TCI and TCW. At the earlier stage of transition, TCI (TCW) underwent ET as it is affected by the incursion of cold air descending from the middle and high levels when moving into the mid-latitude baro clinic zone. Following further incursion of cold air and the intense development of a low-level baroclinic frontal zone (mild cold air only invades into the peripheral circulation of TCW whose baroclinic frontal zone is not obvious) after Te, TCI (TCW) exhibits the strengthened (reduced) low-level convergence and significantly (mildly) enhanced upward motion, thus its low-level cyclone evolves as well (does not evolve). Besides, the upward transport of TCI's *KD* causes the upper-level trough to develop (the upward transport of TCW's *KD* is not evident and the upper-level though does not develop). At this moment, TCI (TCW) is located in the divergence region at the right of the entry to a high-level jet stream and acquires strong *KD*, parts of which converts into *KR* at high levels. Furthermore, the growth (dissipation) of the generation of kinetic energy by rotational wind in TCI (TCW) at high levels is favorable (unfavorable) for TCI's (TCW's) maintenance, which is affected by the strong (weak) upper-level trough. The intensification of TCI during ET is a process in which the low-level cyclone and the upper-level trough help each other in mutual development.

The evolution of ET is a very complex four-dimensional process and can be associated with multiple factors and multiscale interactions. Although a preliminary composite analysis has been done on the differences of atmospheric environment and the kinetic energy budget has been computed to study the TCI and TCW in this paper, further work is still needed. The influences of the allocation between the TC and the westerly trough, the intensity of the TC itself and the intensity of cold air during ET are still unclear, which awaits more numerical work in the future.

REFERENCES:

[1] JONES S C, HARR P A, ABRAHAM J, et al. The extratropical transition of tropical cyclones: forecast challenges, current understanding, and future directions [J]. Wea Forecasting, 2003, 18(6): 1 052-1 092.

[2] ZHAO Yu, WU Zeng-mao, LIU Shi-jun, et al. Potential vorticity analysis of an torrential rain triggered by a neutercane in Shandong Province [J]. J Trop Meteorol, 2005, 21 (1): 34-43 (in Chinese).

[3] LIANG Jun, CHEN Lian-shou, LI Ying, et al. Impacts of two tropical cyclones experiencing extratropical transition during northward progression on the rainfall of Liaodong Peninsula [J]. J Trop Meteorol, 2009, 15(1): 49-53.

[4] FOLEY G R, HANSTRUM B N. The capture of tropical cyclones by cold fronts off the west coast of Australia [J]. Wea Forecasting, 1994, 9(4): 577-592.

[5] KLEIN P M, HARR P A, ELSBERRY R L. Extratropical transition of Western North Pacific tropical cyclones: An overview and conceptual model of the transformation stage [J]. Wea Forecasting, 2000, 15(4): 373-395.

[6] HARR P A, ELSBERRY R L. Extratropical transition of tropical cyclones over the Western North Pacific Part Ⅰ: Evolution of structural characteristics during the transition process [J]. Mon Wea Rev, 2000, 128(8): 2 613-2 633.

[7] HARR P A, ELSBERRY R L. Extratropical transition of tropical cyclones over the Western North Pacific Part Ⅱ: The impact of midlatitude circulation characteristics [J]. Mon Wea Rev, 2000, 128(8): 2 634-2 653.

[8] RITCHIE E A, ELSBERRY R L. Simulations of the extratropical transition of tropical cyclones: Phasing between the upper-level trough and tropical cyclones [J]. Mon Wea Rev, 2007, 135(2): 862-876.

[9] DUAN Yi-hong, YU Hui, WU Rong-sheng. Review of the research in the intensity change of tropical cyclone [J]. Acta Meteorol Sinica, 2005, 63(5): 636-645 (in Chinese).

[10] ZHU Pei-jun, ZHENG Yong-guang, TAO Zu-yu. Analysis of extratropical transition of tropical cyclone over mainland China [J]. J Trop Meteorol, 2003, 9(2): 152-157.

[11] ZHU Pei-jun, ZHENG Yong-guang, TAO Zu-yu. Simulation on reintensification of Typhoon Winnie (1997) during extratopical transition [J]. Acta Meteorol Sinica, 2009, 67(5): 736-749 (in Chinese).

[12] LI Ying, CHEN Lian-shou, LEI Xiao-tu. Moisture potential vorticity analysis on the extratropical transition processes of Winnie (1997) and Bilis (2000) [J]. J Trop Meteorol, 2005, 21(2): 142-152 (in Chinese).

[13] LI Ying, CHEN Lian-shou, LEI Xiao-tu. Numerical study on impacts of upper-level westerly trough on the extratropical transition process of typhoon Winnie (1997)[J]. Acta Meteorol Sinica, 2006, 64(5): 552-563 (in Chinese).

[14] LI Ying, CHEN Lian-shou, LEI Xiao-tu. Frontogenesis in the circulation of typhoon Winnie (1997) during its extratropical transition process [J]. Chin J Atmos Sci, 2008, 32(3): 629-639 (in Chinese).

[15] ZHONG Ying-min, XU Ming, WANG Yuan. Spatio-temporal distributive characteristics of extratropically transitioning tropical cyclones over the Northwest Pacific [J]. Acta Meteorol Sinica, 2009, 67(5): 697-707 (in Chinese).

[16] ONOGI K,TSUTSNI J,KOIDE H, et al. The JRA-25 reanalysis [J]. J Meteorol Soc Jpn, 2007, 85(3): 369-432.

[17] LI Ying, CHEN Lian-shou, WANG Ji-zhi. The diagnostic analysis on the characteristics of large scale circulation corresponding to the sustaining and decaying of tropical cyclone after its landfall [J]. Acta Meteorol Sinica, 2004, 62(2): 167-179 (in Chinese).

[18] HART R E. A cyclone phase space derived from thermal wind and thermal asymmetry [J]. Mon Wea Rev, 2003, 131(4): 585-616.

[19] EVANS J L, HART R E. Objective indicators of the life cycle evolution of extratropical transition for Atlantic tropical cyclones [J]. Mon Wea Rev, 2003, 131 (4): 909-925.

[20] ZHANG Ying-xin, ZHANG Shou-bao, WANG Fu-xia. Application of an objective discriminating method in the evolution of tropical cyclone "Haima" during extratropical transition [J]. J Trop Meteorol, 2008, 14(2): 149-152.

[21] WANG Yuan, SONG Jin-jie. Some characteristics on extratropical transition of tropical cyclones over the Western North Pacific [C]//Chinese Meteorological Society. The 2009 Cross-Strait Seminar on Meteorological Science and Technology. Beijing: China Meteorological Press, 2009: 9-16 (in Chinese).

[22] BOSART L F, VELDEN C S, BRACKEN W E, et al. Environmental influences on the rapid intensifi cation stage Hurricane Opal (1995) over the Gulf of Mexico [J]. Mon Wea Rev, 1998, 128(2): 322-352.

[23] PEARCE R P. The design and interpretation of diagnostic studies of synoptic scale atmospheric system [J]. Quart J Roy Meteor Soc, 1974, 100(425): 265-285.

[24] ENDLICH R M. An iterative method for altering the kinetic properties of wind fields [J]. J Appl Meteorol, 1967, 6(5): 837-844.

[25] BUECHLER D E, FUELBERG H E. Budgets of divergent and rotational Kinetic Energy during two periods of intense convection [J]. Mon Wea Rev, 1986, 114 (1): 95-114.

Citation: LI Kan and XU Hai-ming. Comparative analysis of the intensifying and weakening landfall tropical cyclones during extratropical transition over China [J]. J Trop Meteorol, 2015, 21(1): 23-33.